

# Photovoltaic Synchronous Generator: Architecture and Control Strategy for a Grid-Forming PV Energy System

Xiangjun Quan<sup>ID</sup>, Member, IEEE, Ruiyang Yu, Xin Zhao, Yang Lei<sup>ID</sup>, Tianxiang Chen, Student Member, IEEE, Chengjing Li, Student Member, IEEE, and Alex Q. Huang<sup>ID</sup>, Fellow, IEEE

**Abstract**—Transforming a conventional photovoltaic (PV) energy system from a grid-following to a grid-forming system is necessary when PV power generation is dominating the generation mix and for replacing traditional synchronous generators (SGs). The grid-forming PV energy system can provide frequency support functionality, which is vital for the stability of the power grid. This article presents a novel ac coupled solution that transforms an existing grid-following PV system to a grid-forming one without any hardware and software modification of the PV inverter. The resulting system, the PVSG, is achieved by an ac coupled supercapacitor-based energy storage system (ESS). The novel control of the PVSG is implemented in the ESS side. The novel control scheme includes fast and slow instantaneous power controls. The fast-instantaneous power flow control is fulfilled by the dc-link voltage control and ac voltage control. The cascaded voltage source controls enable fast-instantaneous power balance, while a slow instantaneous power control is used to implement inertia and grid synchronization. Two important fundamental functions are realized in the PVSG. The first one is the frequency inertia to resist the grid frequency variation where  $d\phi/dt$ -based power control is achieved; the second one is the inertia against the PV intermittent power. The correctness and the effectiveness of the proposed PVSG are experimentally validated in a 480 V PVSG prototype with a TMS320F28379D DSP controller.

**Index Terms**—Current controlled, energy storage system (ESS), grid-forming inverter, inertia, inverter control, power control, photovoltaic (PV) synchronous generator (SG)(PVSG), supercapacitors (SCs), virtual SG(VSG), voltage controlled.

## I. INTRODUCTION

**G**RID-CONNECTED inverters, the interface between the distributed generation (DG) and the grid, can be categorized as grid-following inverters and grid-forming inverters [1]. The grid-following inverters generally are

Manuscript received June 14, 2019; revised August 24, 2019 and October 21, 2019; accepted October 26, 2019. Date of publication November 13, 2019; date of current version May 6, 2020. This work was supported in part by Duke Energy through the Center for Advanced Power Engineering Research (CAPER) and in part by The State Grid Corporation Project (Research of improvement of power supply quality and reduction of loss for poverty alleviation PV distribution based on adaptive control). Recommended for publication by Associate Editor Lennart Harnefors. (*Corresponding author: Xiangjun Quan*).

X. Quan is with the Department of Electrical Engineering, Southeast University, Nanjing 210018, China (e-mail: xquan@seu.edu.cn).

R. Yu, X. Zhao, Y. Lei, T. Chen, C. Li, and A. Q. Huang are with the Department of Electrical and Computer Engineering, University of Texas at Austin, Austin, TX 78712 USA (e-mail: aqhuang@utexas.edu).

Color versions of one or more of the figures in this article are available online at <http://ieeexplore.ieee.org>.

Digital Object Identifier 10.1109/JESTPE.2019.2953178

current-controlled (CC), while the grid-forming inverters are usually voltage-controlled (VC). The CC grid-following inverters are widely used in DG applications, such as PV inverters, due to its advantages of fast dynamics and well-developed knowledge base. However, nowadays, the VC grid-forming inverter, due to its attractive merit of voltage source characteristic, has attracted more interest than the CC inverters [2]. The most important reason is the fact that the grid-forming inverters, within their physical limitations, can supply a more convenient and stable way to realize grid support functionalities, including but not limited to inertia support, primary and secondary frequency regulations, and black start [2].

Frequency control is very important for the stability of ac systems since the grid frequency reveals the degree of balancing between generations and demands. During a frequency event, a primary frequency control is always required to arrest the fast frequency decline in the time-scale of seconds or minutes [3]. The function of the primary frequency control is typically achieved by inertia supply and frequency droop [4]. For synchronous generators (SGs), the kinetic energy stored in their rotors serve as the inertia energy to fight against frequency deviations, thus providing sufficient time for the frequency droop control to come into effect. For grid-connected VC inverters, the inertia should include two aspects. The first one is the inherent frequency inertia. This requires that the frequency of the VC inverter should vary slowly when its output power changes. This aspect can be realized by the well-known virtual SG (VSG) control where the swing equation is emulated [5]–[9]. The second inertia function is the inertia support for the grid. In this condition, the inertia support requires a very fast but short duration active power injection/absorption to/from the grid. Two functions should be performed for this inertia support. First, when the grid frequency changes, the inverter should supplies/absorbs active power to resist the frequency change; second, if a pulsating power appears due to the PV intermittence, the inverter should filter the pulsating power to avoid the pulsating power into or from the grid. The frequency droop is a longer time constant active power support function to restore the grid frequency with static-state error, which needs more energies than inertia support. Based on a well-tuned inner voltage control loop, the primary frequency control can be realized by the outer loop power controls. The controls can be the VSG control [5]–[8]

or the droop control [10], [11]. Although the droop control was originally used for power sharing, it is indicated in [11] and [12] that the droop control is equivalent to the VSG from the inertia emulation point of view. Moreover, since the frequency is used as the control variable to regulate the active power, these power controls are also called synchronous power control (SPC) in [13]–[16].

From the perspective of energy demand, the realization of the inertia-support control for the VC inverter requires energy storage. Sometimes, the dc-link capacitor of the inverters can serve as the energy storage for inertia support; however, the dc-link voltage has to be allowed to operate with a large variation [3], [17]–[19]. Considering the pulsating power characteristic of the inertia, the supercapacitor (SC), as a power-type energy storage, is more suitable for the inertia emulation with additional benefits of high-power density and longer lifetime [3]. The batteries are always used to remedy the energy density deficiency of the SC to realize the droop control. Used together will result in a hybrid energy storage system (HESS) suitable for a complete primary frequency control function [20]–[22].

With the increasing penetration of photovoltaic (PV) generation in power grids, the utility companies are now demanding frequency regulation by future PV plants, in the form of either the primary or secondary frequency regulation, or just the inertia support [23]. The development of novel frequency control for the PV system is therefore flourishing, and a number of past works have focused on the PV inverter with inertia supply [24]–[27]. The reported realization methods consist of nonmaximum power point tracking (MPPT) operation [24], using dc-link capacitor [17], [25], or using battery integrated on the dc side [26] or ac side [27]. These methods are suitable for developing a completely new PV inverter system, with both hardware and software changes. Although these methods perform very well, they do not work with the existing grid-following PV plants that are already deployed. How to transform the existing PV systems from grid-following into grid-forming operation with minimum cost is therefore very meaningful. To this end, this article will present an SC-based ac-coupled solution to provide the inertia for the grid. The grid-following PV systems are just connected to the SC-based grid-forming inverter in parallel on the ac side and the PV inverter hardware and software do not need to change. The overall system then operates like a VSG with inertia, and is called PVSG. The proposed solution also does not require the power generation information of the PV.

For the realization of inertia support, the reported control methods are also diverse. The early works mainly focused on the power inertia emulation on the ac side under the assumption that there is an ideal voltage source on the dc side [5]–[7]. These controls were usually originated from emulating the well-known swing equation. In [13]–[16], the power control was extracted as different compact transfer functions (TFs), which can realize the droop control. Lately, when the inertia is emulated by the energy stored in the dc-link capacitor, the inertia emulation loop was usually added to the dc-link voltage control [17]–[19], [21], [26]. The difference for [21] is that the dc-link capacitor was using SC to obtain larger inertia.

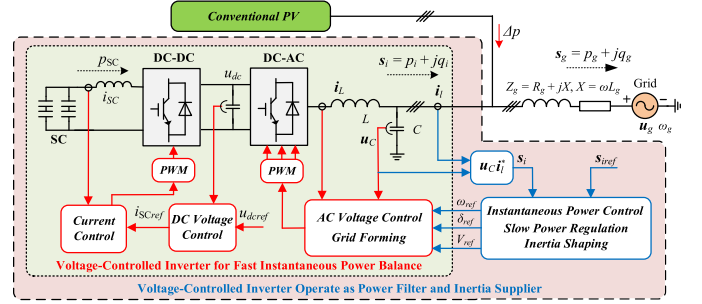


Fig. 1. Illustration of the proposed PVSG by paralleled grid-forming inverter.

As previously stated, these methods are suitable for new PV inverter design; hence they are hard to apply to the already deployed PV inverters. Furthermore, very recently, the frequency-derivative ( $d\delta/dt$ )-based controls are proposed in [28] and [29] to realize the inertia support. However, they are applied to the grid-following inverter where the grid synchronization is required.

In this article, an SC-based inertia solution for the existed PV system is established using an ac coupled inverter that includes a cascaded dc–dc converter and a dc–ac inverter. The SC system is placed in parallel at the ac side with a traditional grid-following PV inverter, and the grid-forming control is implemented in the SC inverter. Then, the whole system, which includes the added SC inverter and the traditional PV inverter, immediately operates as PVSG with inertia, and the intermittence solar power is filtered automatically by the added SC inverter. The inertia is realized by the control of the paralleled SC inverter. The instantaneous power flow of the whole system is controlled by different controllers with different time scales. The fast-instantaneous power flow, which rapidly responds to the intermittent power or grid frequency change, is realized by the inner voltage loop, while the slow instantaneous power flow is regulated by the power loop to implement the inertia support. The proposed inertia solution has two aspects: 1) the SC-based inverter can provide the inertia support to resist the frequency derivation when grid frequency changes. A frequency-derivative-based grid-forming control is proposed. This aspect is defined as frequency inertia in this article, and 2) the PVSG will automatically filter the fluctuation power from the PV so that the power flowing into the grid is smoothed. In this manner, the converter actually operates like a power filter to filter the pulsating power [20]–[22]. This aspect is called a power filter in the article. Furthermore, excellent power tracking control is also achieved.

## II. PVSG ARCHITECTURE

Fig. 1 displays the schematic illustration of the proposed PVSG whose equivalent circuit diagram is shown in Fig. 2. The PVSG includes a grid-following PV (and/or load) in parallel with a grid-forming inverter with SC on the dc side. The control of the PV is a standard grid-following MPPT-controlled inverter system. PVSG controls are implemented in the SC inverter which can be further divided into two parts. The first one is the fundamental voltage and current

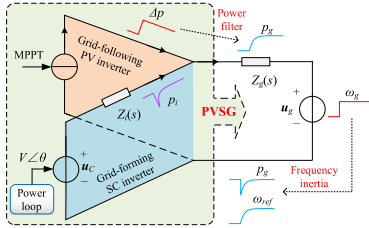


Fig. 2. Equivalent circuit diagram of the proposed PVSG and the functionality illustration of the power filter and frequency inertia.

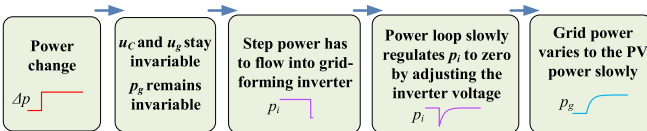
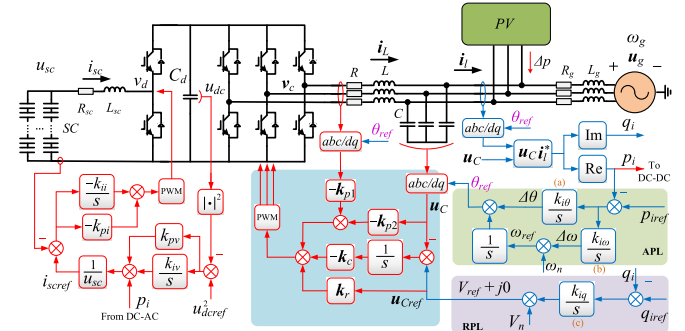


Fig. 3. Power response mechanism to the fluctuation power of the proposed PVSG.

control with a fast dynamic response which achieves the automatic and fast response to the power intermittence and grid frequency variations, as shown by red parts in Fig. 1. The second part implements the slow power control to emulate the inertia, hence achieving power filter and frequency inertia, as shown by the blue parts in Fig. 1.

The proposed inertia solution includes frequency inertia and power filter as demonstrated in Fig. 2. These two functions are used to alleviate the power demand of kinetic energy of SG in event of power and frequency variations. Therefore, they need a very fast and short time active power injection/absorbing to/from the grid when PV power or frequency changes suddenly. To this end, the response of the grid-forming inverter should be as fast as possible to avoid the requirement of step power from the grid. As shown in Fig. 2, the conventional grid-following PV system achieves the MPPT control, while the added inverter operates as a voltage source whose amplitude and frequency are adjusted by the power loop. The approximate zero impedance is designed for the grid-forming inverter to guarantee  $Z_i(s) \ll Z_g(s)$  around the fundamental frequency (the harmonic component will be considered in future work). The PV system is paralleled to the grid-forming inverter, then the whole system, namely PVSG, is connected to the grid with an inductor  $L_g$ . In this condition, the fast power response of the PVSG is ensured by the physical mechanism of the parallel architecture.

The detailed response mechanism for the power fluctuation is illustrated in Fig. 3. The grid power  $p_g$  depends on the voltages of the two sides of the inductor  $L_g$ ; one is the grid voltage, and the other one is the inverter voltage. When a pulsating power  $\Delta p$ , as shown in 3, is generated by the PV, this pulsating power has to flow into the grid-forming inverter first because the frequency and phase of the inverter remain invariable at that moment, and then the grid power must be invariable due to the invariable voltages of two sides of the inductor. This physical mechanism, which is the intrinsic propriety of the voltage source, guarantees that the pulsating power automatically flows into the SC inverter side, hence avoiding negative impacts on the grid. After that,



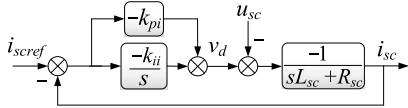


Fig. 5. Control block diagram of the SC current loop.

APL will avoid the mutation of the inverter frequency and phase, consequently the power response mechanism described in Fig. 3 is feasible. The fluctuation power will be absorbed by the SC via the grid-forming inverter, then after a while (this time depends on the integrator gains), the inverter power is forced to the reference  $p_{\text{ref}}$  by the APL. Once  $p_{\text{ref}}$  is not variable, the pulsating power gradually flows into the grid with the dynamic shaped by the APL, since it has the following relationship

$$p_g = p_i + \Delta p. \quad (1)$$

The tracking dynamic process of the inverter power  $p_i$ , which is the dynamic process of how pulsating power goes into the grid, depends on the power control gains. Hence, the power filter function can be achieved by the APL with well-designed gains.

It is worth mentioning that the proposed PVSG solution is independent of the paralleled PV. Because, from the perspective of the paralleled inertia VC inverter, the PV is treated as a power disturbance. The power information of the paralleled PV is not required for the PVSG operation. If the conventional PV is connected to the terminal of the paralleled inertia supplier, the whole system will automatically perform the output characteristic of an SG. This is why it is called a PVSG.

### III. CONTROL FOR FAST POWER FLOW

#### A. DC-DC Control

The dc-link voltage is controlled by the SC, so that the SC can respond quickly to the active power demand, which is reflected by the dc-link voltage. The dc-side control is composed of an outer dc-link voltage loop and inner SC current loop, as shown in Fig. 4. The inner SC current loop is necessary since the SC also needs to be charged at the startup phase when the SC voltage is zero. When the dual-loop structure is adopted, some bandwidth of the dc-link voltage loop has to be traded off for the decoupling of the SC current loop. This tradeoff is not desirable for the requirement of the fast-dynamic response. Hence, the ac power feedforward is designed to improve the dynamic response.

The SC current control block diagram is shown in Fig. 5. The switching frequency averaged model is adopted. The disturbance of the SC voltage can be neglected because it changes slowly due to the large capacitance value. In this condition, the closed-loop TF of the current loop is

$$i_{\text{sc}} = G_{\text{cr}}(s)i_{\text{scref}} = \frac{k_{pi}s + k_{ii}}{L_{\text{sc}}s^2 + (R_{\text{sc}} + k_{pi})s + k_{ii}}i_{\text{scref}}. \quad (2)$$

The reference tracking gain  $G_{\text{cr}}(s)$  is a second-order TF with a zero. For such a system, when it is underdamped, which means it has a pair of conjugated roots, the zero always aggravates the oscillation in the dynamic

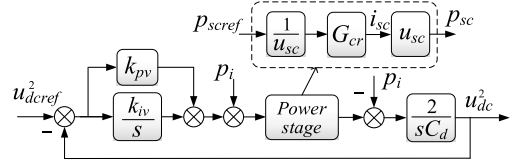


Fig. 6. Control block diagram of the dc-link voltage loop.

process [30]. Moreover, according to the system requirement of the fast-dynamic response, the bandwidth should be as high as possible. Hence, the PI parameters can be determined by selecting the characteristic roots of the TF with higher damping oscillation frequency and critical damping factor.

The proposed dc-link voltage control is based on a power model. The power model of the dc-link with a capacitor  $C_d$  can be expressed as (the instantaneous power of the filters is neglected)

$$\frac{1}{2}C_d \frac{du_{\text{dc}}^2}{dt} = p_{\text{sc}} - p_i. \quad (3)$$

Fig. 6 shows the power-model-based dc-link voltage control diagram. At least one-fifth of the current loop bandwidth should be designed for the outer loop, so that the inner power stage can be treated as a unity link. The ac power is used as the feedforward to improve dynamic response. Then closed-loop TF of the dc-link voltage control is

$$u_{\text{dc}}^2 = G_{\text{vr}}(s)u_{\text{dcref}}^2 = \frac{2k_{pv}s + 2k_{iv}}{C_d s^2 + 2k_{pv}s + 2k_{iv}}u_{\text{dcref}}^2 \quad (4)$$

which can also be designed by placing the roots to select the PI parameters.

#### B. DC-AC Control

To design the voltage tracking control of the inverter, the complex-state-space-based model of the three-phase inverter with the  $LC$  filter is first given by

$$\begin{cases} \dot{\mathbf{x}}_p = \mathbf{A}_p \mathbf{x}_p + \mathbf{B}_{p1} \mathbf{v}_c + \mathbf{B}_{p2} \mathbf{i}_l \\ \mathbf{y} = \mathbf{C}_p \mathbf{x}_p. \end{cases} \quad (5)$$

In this model, the complex state variables  $\mathbf{x}_p: [\mathbf{i}_L \ \mathbf{u}_C]^T = [i_{Ld} + ji_{Lq} \ u_{Cd} + ju_{Cq}]^T$  denote the inductor current and the capacitor voltage, and  $\mathbf{i}_l = i_{ld} + ji_{lq}$  represents the disturbance from the outside. The middle point voltage of the bridge leg  $\mathbf{v}_c = \mathbf{v}_{cd} + j\mathbf{v}_{cq}$  is the control input. By defining  $a_1 = 1/L$  and  $a_2 = 1/C$ , the matrices in (5) can be easily derived

$$\begin{aligned} \mathbf{A}_p &= \begin{bmatrix} -Ra_1 - j\omega & -a_1 \\ a_2 & -j\omega \end{bmatrix}, \quad \mathbf{B}_{p1} = \begin{bmatrix} a_1 \\ 0 \end{bmatrix} \\ \mathbf{B}_{p2} &= \begin{bmatrix} 0 \\ -a_2 \end{bmatrix}, \quad \mathbf{C}_p = \begin{bmatrix} 0 & 1 \end{bmatrix}. \end{aligned} \quad (6)$$

Then, the state variable of the integrator is defined as

$$\dot{\mathbf{x}}_c = \mathbf{e}_c = \mathbf{u}_{\text{Cref}} - \mathbf{u}_C. \quad (7)$$

The open-loop system representation of the ac voltage control scheme shown in Fig. 4 can be formulated as

$$\begin{cases} \dot{\mathbf{x}} = \begin{bmatrix} -Ra_1 - j\omega & -a_1 & 0 \\ a_2 & -j\omega & 0 \\ 0 & -1 & 0 \end{bmatrix} \mathbf{x} + \begin{bmatrix} a_1 \\ 0 \\ 0 \end{bmatrix} \mathbf{v}_c \\ + \begin{bmatrix} 0 \\ -a_2 \\ 0 \end{bmatrix} \mathbf{i}_l + \begin{bmatrix} 0 \\ 0 \\ 1 \end{bmatrix} \mathbf{u}_{Cref} \\ \mathbf{y} = \mathbf{u}_C = \mathbf{Cx} = [0 \ 1 \ 0] \mathbf{x} \end{cases} \quad (8)$$

where  $\mathbf{x} = [\mathbf{x}_p \ \mathbf{x}_c]^T = [\mathbf{i}_L \ \mathbf{u}_C \ \mathbf{x}_c]^T$  represents the augmented state variables. The proposed capacitor voltage control law is

$$\mathbf{v}_c = -\mathbf{k}_{p1}\mathbf{i}_L - \mathbf{k}_{p2}\mathbf{u}_C - \mathbf{k}_c\mathbf{x}_c + \mathbf{k}_d\mathbf{i}_l + \mathbf{k}_r\mathbf{u}_{Cref}. \quad (9)$$

Then the closed-loop system is

$$\dot{\mathbf{x}}_{ab} = \mathbf{A}_c \mathbf{x} + \mathbf{B}_{2c}\mathbf{i}_l + \mathbf{B}_{rc}\mathbf{y}_{Cref} \quad (10)$$

where

$$\mathbf{A}_c = \begin{bmatrix} -Ra_1 - a_1\mathbf{k}_{p1} - j\omega & -a_1 - a_1\mathbf{k}_{p2} & -a_1\mathbf{k}_c \\ a_2 & -j\omega & 0 \\ 0 & -1 & 0 \end{bmatrix}$$

$\mathbf{B}_{2c} = [a_1\mathbf{k}_d \ -a_2 \ 0]^T$ ,  $\mathbf{B}_{rc} = [a_1\mathbf{k}_r \ 0 \ 1]^T$ . The state feedback gain  $\mathbf{K} = -[\mathbf{k}_{p1} \ \mathbf{k}_{p2} \ \mathbf{k}_c]$  can be designed by the well-known pole placement method (Ackermann algorithm [31]), and then the feedforward  $\mathbf{k}_d$  and  $\mathbf{k}_r$  can be designed by pole-zero cancellation [32], since the zeros of the system is independently related with  $\mathbf{k}_d$  and  $\mathbf{k}_r$  based on the closed-loop TF

$$\begin{aligned} \mathbf{u}_C &= \mathbf{C}(s\mathbf{I} - \mathbf{A}_c)^{-1}(\mathbf{B}_{2c}\mathbf{i}_l + \mathbf{B}_{rc}\mathbf{u}_{Cref}) \\ &= \mathbf{G}_d\mathbf{i}_l + \mathbf{G}_r\mathbf{y}_{ref} = \frac{\mathbf{Z}_d(s)\mathbf{i}_l + \mathbf{Z}_r(s)\mathbf{u}_{Cref}}{(s - p_d)(s - p_n)(s - p_n^*)} \end{aligned} \quad (11)$$

where

$$\mathbf{Z}_d(s) = a_2s(a_1\mathbf{k}_d - s - j\omega - a_1R - a_1\mathbf{k}_{p1}) \quad (12)$$

$$\mathbf{Z}_r(s) = a_1a_2(\mathbf{k}_{rs} - \mathbf{k}_c) \quad (13)$$

and  $p_d$  is the dominant pole,  $p_n, p_n^*$  are two nondominant poles determined by the pole placement method. By tuning  $\mathbf{k}_d$  and  $\mathbf{k}_r$ , the zeros of  $\mathbf{Z}_d$  and  $\mathbf{Z}_r$  can be designed to equal  $p_d$ . Consequently, the fast-dynamic response can be achieved by the proposed control. Moreover, the impedance shaped by this control algorithm is much smaller than the grid impedance around 0 Hz (represents the fundamental component in  $dq$  frame), as shown in Fig. 7. The inverter impedance increases from 200 to 2000 Hz, which will affect the harmonic power sharing. This problem can be resolved via configuring the multiple resonant controllers for the voltage control, which will be further studied in the future work.

For the proposed ac coupled solution, the fast response is used to compensate the pulsating power demand of the grid, thus avoiding the pulsating power requirement of the grid. Hence, from this viewpoint, the response speed of the grid-forming inverter should be as fast as possible. However, in practice, first, the bandwidth of the ac voltage control loop cannot be infinite, and also high bandwidth may cause the risk

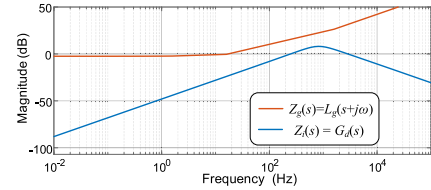


Fig. 7. Impedances of the inverter and grid.

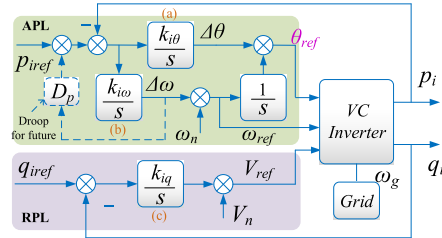


Fig. 8. Illustration of the power control block. (a)–(c) Labels of the three integrators.

of stability and noise issue; on the other hand, the response speed cannot be designed too slow for the ac voltage loop, and the slow response will interact with the outer power loop; therefore, the response speed of the ac voltage control is better to be designed in 1–5 ms, then the ac voltage loop can be decoupled with the power loop, and also it has a fast response to compensate the step power [32].

Moreover, the issue of current limitation should be considered for the proposed voltage control due to the absence of the current loop. Two approaches can address this problem. The first one is to limit the output of the controller  $\mathbf{v}_c$  according to the relationship between the inductor current and the control voltage. In this way, to determine the safe zone of  $\mathbf{v}_c$ , some extra calculation is required. Second, an equivalent dual-loop control, which includes the current loop, can be derived from the proposed voltage control. The equivalent dual-loop control has the same response with the proposed control, and then the current limit can be imposed on the current reference. For more details concerning the current limitation of the grid-forming inverter, refer to [34] and the references therein.

#### IV. CONTROL FOR SLOW POWER FLOW

Based on the proposed dc–dc and dc–ac voltage control, the cascaded dc and ac voltage sources can respond quickly to the power disturbance from the PV intermittence. If there is no power controller to regulate the phase and amplitude of the inverter voltage, the power shortage yielded by the PV intermittence has to be supplied by the inverter. Considering that the SC is a power-type energy storage, which cannot output power for a long time, hence, the power of the inverter should return to zero after a while. Furthermore, the inverter should also respond to the grid frequency change to supply the frequency inertia. To fulfill the mentioned functions of the power filter and frequency inertia, the power controller is proposed as shown in Fig. 8. The phase and the frequency of the inverter voltage are used to regulate the active power, while the reactive power is controlled by the amplitude of the inverter voltage. Partial content of the power control has

been illustrated in [33], and more comprehensive and detailed illustrations will be demonstrated in Section IV-A–IV-D.

### A. Instantaneous Power Model

The instantaneous power is controlled in this article; hence, the model of the instantaneous power needs to be clarified. The dynamics of the grid inductor can be described under *dq* reference frame as

$$\frac{di_g}{dt} = (-a_3 R_g + j\omega) i_g + a_3 u_C - a_3 u_g \quad (14)$$

where  $a_3 = 1/L_g$ . Considering the grid power  $s_g = p_g + jq_g = u_C i_g^* = U_C I_g e^{j\Delta\varphi}$ , its dynamic process is

$$\frac{ds_g}{dt} = \frac{du_C}{dt} i_g^* + \frac{di_g}{dt} u_C = \frac{du_C}{dt} i_g^* + (-a_3 R_g i_g + a_3 u_C - a_3 u_g)^* u_C. \quad (15)$$

The capacitor voltage has been well controlled with a fast dynamic response, hence in the time scale of the power control, it is considered that  $du_C/dt = 0$ . Thus, (15) becomes

$$\frac{ds_g}{dt} = (-a_3 R_g + j\omega)s_g + a_3 u_C u_C^* - a_3 u_C u_g^* \quad (16)$$

whose steady-state solution is

$$\begin{aligned} s_g &= \frac{u_C u_C^* - u_C u_g^*}{R_g - j\omega L_g} = \frac{U_C^2 - U_C U_g e^{j\Delta\delta}}{R_g - jX} \\ &= \frac{U_C^2 - U_C U_g \cos(\Delta\delta) - j U_C U_g \sin(\Delta\delta)}{R_g - jX} \end{aligned} \quad (17)$$

where  $\Delta\delta$  denotes the phase difference. Evidently, this conclusion is identical to the results of the phasor-based power. Neglecting the resistance, the mathematical models governing  $p$  and  $q$  are expressed with  $\Delta U = U_c - U_g$

$$p_g + jq_g \approx \frac{U_C U_g \Delta\delta}{X} + j \frac{U_C (U_c - U_g)}{X} = A \Delta\delta + j B \Delta U. \quad (18)$$

### B. Active Instantaneous Power Control

To emulate the frequency inertia, the general method is to replicate the swing equation in the active power loop [5]–[8]. However, it is indicated in [13]–[16] that the rigorous replication of the swing equation is not necessary. The inertia emulation with/without inherent droop can be flexibly implemented by different power controllers [13]–[16]. Hence, the proposed APL different from the swing equation is designed as shown in Fig. 8 to realize the required frequency inertia as well as the power filter to the PV system. In Fig. 8, the integrator (a) directly adjusts the phase of the inverter, while the integrator (b) regulates the frequency of the inverter. The whole APL is equivalent to a proportional-integral (PI) control as adopted in [35]. However, a different structure is employed here to acquire a clear frequency signal of  $\Delta\omega$  or  $\omega_{ref}$ . Furthermore, different from the application in [35] where droop control is applied, this article mainly focuses on the inertia realization where the  $df/dt$ -based power control is designed for the grid-forming inverter. Basically, the feature of zero final value of grid frequency response for the proposed APL is utilized to avoid a long-time power output for the SC,

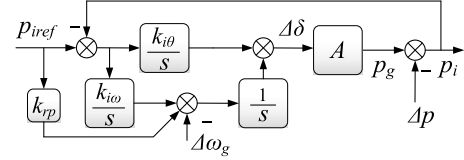


Fig. 9. Small-signal control block diagram of the active power control.

thus achieving the rate of change of frequency (RoCoF)-based power control. Hence, further analyses concerning the inertia and different parameter design methods are performed in this article.

It is worth noting that the droop can be easily implemented without grid frequency information for the proposed control as shown in Fig. 8, because  $\Delta\omega$  is the difference in the grid frequency between the rated frequency  $\omega_n$ , which is  $120\pi$  in this article; hence, it can be used to realize the droop control as shown by the dotted line when the battery is configured. However, only the SC is configured in this article; therefore,  $D_p$  is always zero.

For the proposed PVSG, three fundamental functions are required by the APL: power tracking, frequency inertia, and power filter. To design these functions, the small-signal control block diagram is shown in Fig. 9, where  $k_{rp}$  is added to tune the tracking performance,  $\Delta\omega_g$  denotes the grid frequency variation, and  $\Delta p$  is the power disturbance from PV or loads. As can be seen in Fig. 9, the system has three inputs: power reference  $p_{iref}$ , grid frequency variation  $\Delta\omega_g$ , and power disturbance  $\Delta p$ . Then, the grid power can be described as

$$p_g = G_{rp}(s)p_{iref} + G_{\omega p}(s)\Delta\omega_g + G_{\Delta p}(s)\Delta p. \quad (19)$$

For the application of the proposed PVSG, the power tracking, frequency inertia, and power filter can be shaped by  $G_{rp}(s)$ ,  $G_{\omega p}(s)$ , and  $G_{\Delta p}(s)$ , respectively.

Suppose  $\Delta p = 0$ , the closed-loop transfer function of the system is

$$\begin{aligned} p_g &= p_i = G_{rp}(s)p_{iref} + G_{\omega p}(s)\Delta\omega_g \\ &= \frac{A(k_{i\theta} + k_{rp})s + Ak_{i\omega}}{s^2 + Ak_{i\theta}s + Ak_{i\omega}} p_{iref} + \frac{-As}{s^2 + Ak_{i\theta}s + Ak_{i\omega}} \Delta\omega_g. \end{aligned} \quad (20)$$

As can be seen in (20), instead of the droop coefficient  $D_p$ ,  $k_{i\theta}$  appears as the coefficient of the first-order term  $s$  in the characteristic polynomial. This implies that the introduction of  $k_{i\theta}$  can damp the system to make the system stable.

First, to shape the power tracking performance, rewrite  $G_{rp}(s)$  as

$$G_{rp}(s) = \frac{A(k_{i\theta} + k_{rp})(s + z)}{(s + p_1)(s + p_2)}. \quad (21)$$

Then, it has the relationship between the control parameters and zeros and poles

$$Ak_{i\theta} = p_1 + p_2, \quad Ak_{i\omega} = p_1 p_2, \quad z = \frac{k_{i\omega}}{k_{i\theta} + k_{rp}} \quad (22)$$

which shows that  $k_{rp}$  introduces an adjustable zero. Using this zero can improve the power reference tracking performance.

With the condition of two real poles (which is easy to be designed), we can command  $z = p_2$ ; then  $G_{rp}(s)$  becomes

$$G_{rp}(s) = \frac{A(k_{i\theta} + k_{rp})}{s + p_1} = \frac{p_1}{s + p_1} \quad (23)$$

which is a first-order system, hence it has a good dynamic performance like a first-order system and its settling time can be adjusted by  $T_{Aset} = 4.6/p_1$ . This is important since the good tracking ability of power command is always needed for power scheduling from the superior control layer.

Second, for the frequency inertia, when grid frequency changes, due to the limited energy storage of the SC, the steady-state power output of the inverter should be zero, namely, providing a dynamic power support. Observing  $G_{op}(s)$ , it has  $G_{op}(0) = 0$ , which satisfies the requirement of the final value. In this condition, two indexes during the dynamic process are critical. One is the duration time of the dynamic process; another one is the maximum power during the transient process. The duration time depends on the energy needed by the inertia support, and it can be tuned by the placement of  $p_1$  and  $p_2$ . The maximum power amplitude in the transient process not only concerns the power rating of the SC inverter but also affects the energy required in the duration of the dynamic support. Hence, to explicitly design the maximum power amplitude in the transient process when the grid frequency changes,  $G_{op}(s)$  can be rewritten as

$$G_{op}(j\omega) = \frac{-A j \omega}{-\omega^2 + (p_1 + p_2) j \omega + p_1 p_2}. \quad (24)$$

By computing derivation of (24) with respect to frequency  $\omega$ , the maximum amplitude of (24) can be determined as

$$|G_{op}(j\omega)|_{\max} = \frac{A}{p_1 + p_2} \quad (25)$$

when  $\omega = (p_1 p_2)^{1/2}$ . This value is actually the maximum power during the dynamic response when the grid frequency changes. Correspondingly, the power amplitude is quantitatively determined by  $p_1$  and  $p_2$ . Finally, smaller the poles are designed, the transient time is longer, and the maximum power is bigger, hence the placement of poles should comprehensively consider these two aspects as well as the dynamics of the power tracking control.

Third, the power filter function for the pulsating power disturbance is investigated. In the proposed PVSG, the fluctuation power, which would have occurred by the PV or load, can be treated as power disturbance  $\Delta p$ . Suppose  $p_{iref} = 0$  and  $\Delta\omega_g = 0$ , the power filter performance can be described as

$$\begin{aligned} p_g &= G_{\Delta p}(s)\Delta p = \frac{Ak_{i\theta}s + Ak_{i\omega}}{s^2 + Ak_{i\theta}s + Ak_{i\omega}}\Delta p \\ &= \frac{(p_1 + p_2)s + p_1 p_2}{(s + p_1)(s + p_2)}\Delta p \end{aligned} \quad (26)$$

which is a low-pass filter. Its filtering ability can be designed by  $p_1$  and  $p_2$ . Therefore, with the proposed PVSG design, the PV intermittence can be compensated by the SC inverter. The filter time constant is dependent on  $p_1$  and  $p_2$ .

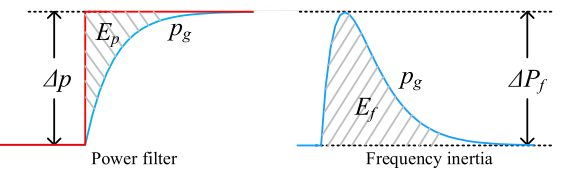


Fig. 10. Illustration of the inertia support for the grid.

### C. Power and Energy Ratings and Inertia Analysis

To investigate the required power and energy of the inertia support, the waveform illustrations of the power filter and frequency inertia support are shown in Fig. 10. For realizing these functions, the area of the shadow region in Fig. 10 represents the energy requirement of the SC. For the power filter, the required energy can be approximated as

$$E_p = \int_0^\infty \Delta p e^{-\frac{t}{\tau}} dt = \Delta p \cdot \tau \quad (27)$$

where the equivalent time constant  $\tau$  is determined by  $p_1$  and  $p_2$ , while the power step amplitude  $\Delta p$  lies on some prior knowledge of the PV intermittence. Obviously, a longer time constant needs more energies for the SC. Moreover, the energy demand of the frequency support is approximated as

$$E_f = \int_0^\infty \Delta P_f \cdot \Delta f \cdot e^{-\frac{t}{\tau}} dt = \Delta P_f \cdot \Delta f \cdot \tau \quad (28)$$

where  $\Delta P_f = 2\pi |G_{op}(j\omega)|_{\max}$  denotes the maximum power amplitude when grid frequency changes 1 Hz,  $\Delta f$  is the grid frequency step in a specific grid condition. According to (25),  $\Delta P_f$  can be tuned by  $p_1$  and  $p_2$ . However, the grid frequency step is generally minor due to the intrinsic inertia of SG. Hence, the determination of  $E_f$  also needs prior knowledge of grid condition. In summary, the power rating is chosen as the maximum of  $\Delta p$  and  $\Delta P_f \Delta f$ . The determination of  $\Delta p$  and  $\Delta f$  needs further information about the PV intermittence and grid condition. While the energy rating can be planned according to the maximum of  $E_p$  and  $E_f$ .

The previous illustration mainly interprets the inertia support from the viewpoint of the time-domain filter performance. It is necessary to further explain how much inertia the proposed control supplies. Suppose that the inertia of the grid is described as

$$J_g \omega_g \frac{d\Delta\omega_g}{dt} = \Delta p_g \quad (29)$$

where  $J_g$  is the moment of inertia,  $\Delta p_g$  (flowing into the grid is set as the positive direction) is the power difference between the grid and load that occurs the frequency deviation. For such a grid,  $\Delta p_g$  generates a RoCoF of  $\Delta p_g/(J_g \omega_g)$ . Then rewriting  $G_{op}(s)$  as

$$p_i = \frac{-As}{s^2 + Ak_{i\theta}s + Ak_{i\omega}} \Delta\omega_g = \frac{-A}{s^2 + Ak_{i\theta}s + Ak_{i\omega}} \frac{d\Delta\omega_g}{dt}. \quad (30)$$

In steady state ( $s = 0$ ), the output power of the SC inverter is proportional to the RoCoF ( $d\omega/dt$ ) with a coefficient of  $k_{pf} = -2\pi/k_{i\omega}$

$$p_i = -\frac{1}{k_{i\omega}} \frac{d\Delta\omega_g}{dt} = -J_{PVSG} \omega_n \frac{d\Delta\omega_g}{dt} \quad (31)$$

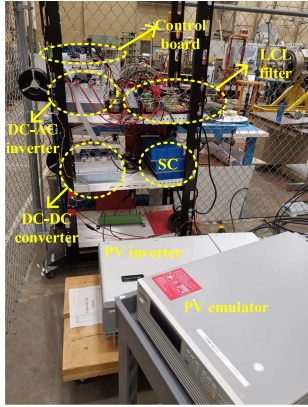


Fig. 11. Experimental setup.

where  $J_{PVSG}$  can be defined as the moment of inertia supplied by the PVSG. Obviously, the power supplied by the PVSG will compensate the power difference  $\Delta p_g$  thus can reduce the RoCoF, because the output power is the feedback of the RoCoF:  $\Delta p_g > 0 \rightarrow d\Delta\omega_g/dt > 0 \rightarrow p_i < 0$  thus  $p_i$  can absorb  $\Delta p_g$  to prevent the frequency reduction. Hence, this article actually realizes the  $df/dt$ -based inertia control for the grid-forming inverter, unlike [28] and [29] where the  $df/dt$ -based control is designed for the grid-following inverter.

Furthermore, from Fig. 8, the frequency inertia of the SC inverter is

$$\frac{1}{k_{i\omega}} \frac{d\Delta\omega}{dt} = J_{PVSG}\omega_n \frac{d\Delta\omega}{dt} = p_{iref} - p_i \quad (32)$$

where the moment of inertia is exactly  $J_{PVSG} = 1/(\omega_n k_{i\omega})$ . According to (22) it has  $J_{PVSG} = 1/(\omega_n k_{i\omega}) = A/(\omega_n p_1 p_2)$ . Finally, to acquire better filter performance and larger inertia, smaller poles should be designed. However, smaller poles also result in bigger power and energy rating. Therefore, a tradeoff between these two aspects has to be made.

#### D. Reactive Instantaneous Power Control

The reactive instantaneous power control is a first-order system with the closed loop of

$$q_g = q_i = G_{rq}(s)q_{iref} + G_{Vq}(s)\Delta V \\ = \frac{Bk_{iq}}{s + Bk_{iq}}q_{iref} + \frac{Bs}{s + Bk_{iq}}\Delta V \quad (33)$$

whose parameter can be designed conveniently. It can also be observed from (33) that when the grid voltage changes, the  $Q$ - $V$  droop is not achieved since  $G_{Vq}(\infty) = 0$ . This droop can be realized simply by means of replacing the integrator with a first-order low pass filter. This part is not the concern of this article; hence, it will not be discussed further.

## V. EXPERIMENTAL VERIFICATION

To experimentally verify the proposed solution, a PVSG experimental setup was developed to implement the proposed control scheme. The setup is displayed in Fig. 11. The dc-dc and da-ac converters employ Applied Power System (APS) IAP 100T120 IGBT power modules. The SC inverter is controlled as a VC inverter by the control algorithm described

TABLE I  
CIRCUIT PARAMETERS OF THE PVSG SYSTEM

Parameter	Value	
$L$	Inductance of AC filter	1 mH
$C$	Capacitance of AC filter	54 $\mu$ F
$R$	Inductor resistance	0.05 $\Omega$
$L_g$	Grid-side inductance	1.5 mH
$L_{sc}$	SC-side inductance	1.8 mH
$SC$	Super capacitance	2 F
$C_d$	DC link capacitance	3300 $\mu$ F
$f_s$	Switching frequency	16,000 Hz
Voltage ph-ph RMS/ frequency	480 V / 60 Hz	
DC link voltage	830 V	

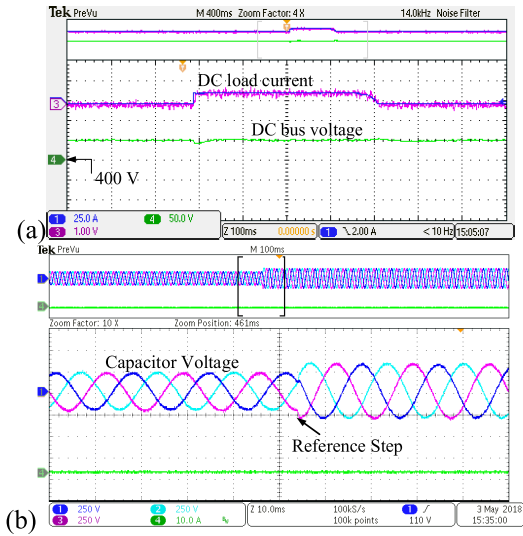


Fig. 12. Experimental results of (a) dc voltage control and (b) ac voltage control.

in Section III. Then the grid-forming inverter is connected to the grid with an inductor, and the power control is realized as illustrated in Section IV. A 32-bit floating-point dual-core TMS320LF28377D DSP is used to realize all the control algorithms in the experiment. Table I lists the system parameters used in this study. A commercial grid-following PV inverter (SUN2000-36-KTL) is connected with the SC inverter. A PV emulator (Chroma 62000H-S) is used as the input of the PV inverter.

#### A. Verification of DC and AC Voltage Control

The dc voltage loop is first experimentally verified. The damping oscillation frequency of the SC current loop is selected as 2000 Hz with a critical damping factor, while the dc-link voltage loop is designed with a damping oscillation frequency of 200 Hz, which is one-tenth of the current loop. The resulted parameters are  $k_{pi} = 19 \Omega$ ,  $k_{ii} = 49317 \Omega \cdot s^{-1}$ ,  $k_{pv} = 1.8 \text{ S}$ ,  $k_{pi} = 491 \text{ S } s^{-1}$ . This value is a little small for the fast dynamic response. To improve the dynamic response of the load change, the ac power feedforward is adopted in the voltage loop. In this experiment, the load power is estimated to realize the power feedforward. As shown in Fig. 12(a), the blue line is the load current captured by the current probe, while the red line is the estimated load current which is used as the power feedforward. The green line shows the dc-link voltage dynamic response of the load change. A good dynamic

response is achieved when the load changes. It means that the dc-link voltage control can respond to the power command to achieve the fast instantaneous power balance.

The tracking control of the ac voltage is also verified, since the tracking ability is important for the outer power loop. The parameters are  $k_p = 5.2446 \Omega$ ,  $k_d = 0.3788$ ,  $k_c = -221.68 + j29.279$ ,  $k_r = 1.3240 + j0.1$ ,  $k_d = 5.124 + j0.374768 \Omega$ . As shown in Fig. 12(b), when the reference of the voltage amplitude stepped down from 100 to 170 V, the ac side capacitor voltage shows an approximately zero dynamic response delay, which is beneficial for the power control.

### B. Verification of Power Control

This section demonstrates the experimental results of the proposed power controller. The reference step and the frequency inertia are tested without load or PV for simplicity. To verify the modeling and design method described in Section IV-B, two example controls are designed to demonstrate different performance for the system with  $U_C = U_g = 170$  V,  $\omega_g = 120\pi$ , and  $X = 0.67854 \Omega$ . The design process is to:

- 1) determine the settling time of the power tracking control  $T_{Aset}$  and the maximum power amplitude  $\Delta P_f$  when grid frequency changes 1 Hz;
- 2) compute the location of poles by:  $p_1 = 4.6/T_{Aset}$  (settling time of first-order systems),  $p_2 = 2\pi A/\Delta P_f - p_1$  according to (25);
- 3) determine the control parameters according to (22)

$$k_{i\theta} = \frac{p_1 + p_2}{A}, \quad k_{i\omega} = \frac{p_1 p_2}{A}, \quad k_{rp} = \frac{k_{i\omega}}{p_2} - k_{i\theta}. \quad (34)$$

Based on the design process, two specifications are designed:  $T_{Aset} = 0.5$  s,  $\Delta P_f = 15$  kW and  $T_{Aset} = 2$  s,  $\Delta P_f = 10$  kW. The resulted control parameters are  $k_{i\theta} = 4.1888e-04 \text{ kg}^{-1} \cdot \text{m}^{-2} \cdot \text{s}^2$ ,  $k_{i\omega} = 0.0025 \text{ kg}^{-1} \cdot \text{m}^{-2} \cdot \text{s}$ ,  $k_{rp} = -2.7432e-04 \text{ kg}^{-1} \cdot \text{m}^{-2} \cdot \text{s}^2$ ,  $J_{PVSG} = 1/(\omega_n k_{i\omega}) = 1.06 \text{ kg} \cdot \text{m}^2$  and  $k_{i\theta} = 6.2832e-04 \text{ kg}^{-1} \cdot \text{m}^{-2} \cdot \text{s}^2$ ,  $k_{i\omega} = 0.0014 \text{ kg}^{-1} \cdot \text{m}^{-2} \cdot \text{s}$ ,  $k_{rp} = -5.9218e-04 \text{ kg}^{-1} \cdot \text{m}^{-2} \cdot \text{s}^2$ ,  $J_{PVSG} = 1/(\omega_n k_{i\omega}) = 1.89 \text{ kg} \cdot \text{m}^2$ .

Fig. 13 shows the performance of the reference step with different settling times. As in Fig. 13(a), the settling time is designed as 0.5 s, when the active power reference steps from 2 to 5 kW and then comes back to zero, the active power can track the power reference perfectly with a good dynamic response and achieve its steady state in 0.5 s, which is conformed to the design target. The current of the SC (blue line) also represents the active power output which verifies the effectiveness of the proposed method. While in Fig. 13(b), the active power reference changes from zero to 5 kW and the settling time is designed as 2 s. The active power response in Fig. 13(b) shows that the zero-static-state-error active power control is achieved with the settling time of 2 s, and the dynamic response is also very good due to the first-order system behaviors realized by the proposed power controller. The current of the SC keeps increasing in Fig. 13(b), because the SC voltage is lower than Fig. 13(a); consequently, the SC

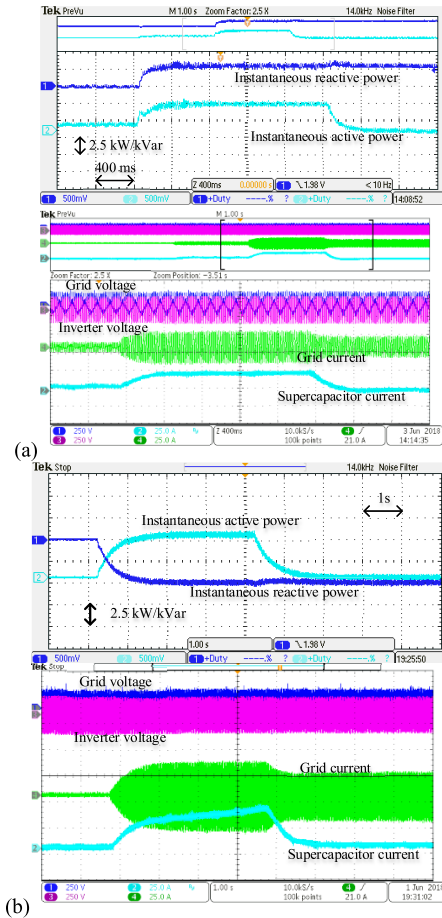


Fig. 13. Experimental results for reference step: (a)  $T_{Aset} = 0.5$  s; (b)  $T_{Aset} = 2$  s.

voltage decreased faster and SC current increased noticeably to sustain the constant active power output.

Fig. 14 shows the response of the grid frequency change for 0.5 s-15 kW/Hz and 2 s-10 kW/Hz designs. Fig. 14(a) shows that when the grid frequency decreased 0.5 Hz, the inverter injects active power immediately to provide the inertia support. This active power attempts to mitigate the power requirement from the inertia kinetic energy stored in their rotors. When the grid frequency steps 0.5 Hz, which means the power of the grid surplus, hence, the inverter absorbs active power immediately. The maximum power is approximate 7.5 kW during the dynamic process and the transient time is 0.5 s, which accords with the design specification. The frequency of the inverter also automatically synchronizes to the grid in 0.5 s. The displayed frequency information is derived from the power controller. The results prove that the predefined specifications are achieved and the proposed control is correct. For the 2 s-10 kW/Hz design, its response to the grid frequency step is displayed in Fig. 14(b). When grid frequency steps to  $-0.5$  Hz, the inverter generates a maximum power injection of 5 kW, and also when the grid frequency increases to 0.5 Hz, the inverter absorbs power from the grid with 5-kW maximum power amplitude. The dynamic time for the synchronization and output power is 2 s, which is the designed inertia time. The experimental results in this section mainly prove that the proposed power modeling and control method is correct

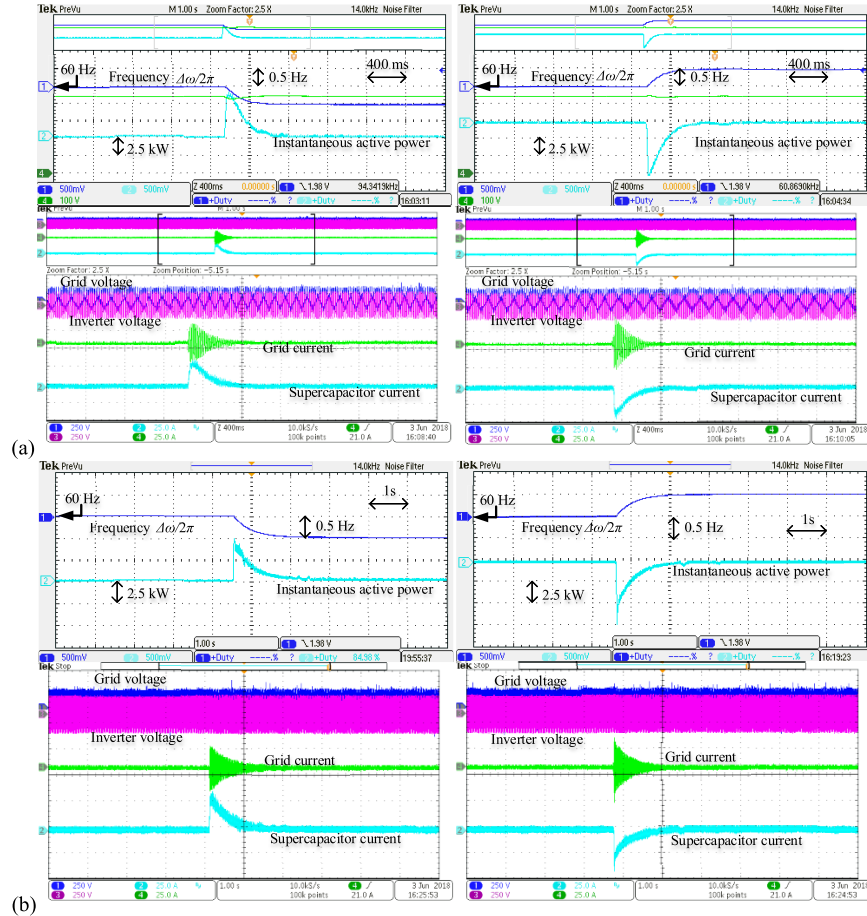


Fig. 14. Experimental results for grid frequency change: (a)  $T_{Aset} = 0.5$  s,  $\Delta P_f = 15$  kW; (b)  $T_{Aset} = 2$  s,  $\Delta P_f = 10$  kW.

and effective. Consequently, the concrete functions of the frequency inertia and power filter can be realized by the proposed PVSG.

To highlight the improvement of the proposed control, the  $df/dt$  power control is experimentally verified and a comparison between the proposed power control and the PI-based control is conducted. The poles are selected as  $p_1 = p_2 = 3$ , which results in  $k_{i\theta} = 9.43e-05 \text{ kg}^{-1} \cdot \text{m}^{-2} \cdot \text{s}^2$ ,  $k_{i\omega} = 1.41e-04 \text{ kg}^{-1} \cdot \text{m}^{-2} \cdot \text{s}$ ,  $k_{rp} = -4.71e-05 \text{ kg}^{-1} \cdot \text{m}^{-2} \cdot \text{s}^2$ ,  $J_{PVSG} = 1/(\omega_n k_{i\omega}) = 18 \text{ kg} \cdot \text{m}^2$  for  $U_C = U_g = 170 \text{ V}$ ,  $\omega_g = 120\pi$ , and  $X = 0.67854 \Omega$ . Then according to (31),  $k_{pf} = -2\pi/k_{i\omega} = -4.44e+04 \text{ W/(Hz/s)}$ . As shown in Fig. 15, when the grid frequency ramps with a slope of  $-0.1$  and  $0.05 \text{ Hz/s}$ , the PVSG injects  $4.4 \text{ kW}$  and absorbs  $2.2\text{-kW}$  active power. The frequency-derivative-based power control is clearly realized for the grid-forming inverter. Furthermore, in Fig. 16, the proposed power controller is experimentally compared with the PI-based power control with the power reference step. As shown in Fig. 16(a), the proposed power controller behaves like a first-order system without any overshoot, while the PI-based power control manifests an obvious overshoot on the active power response.

### C. Grid-Connected PVSG Test Results

In this section, the functions of the frequency inertia and power filter will be verified by means of connecting to the

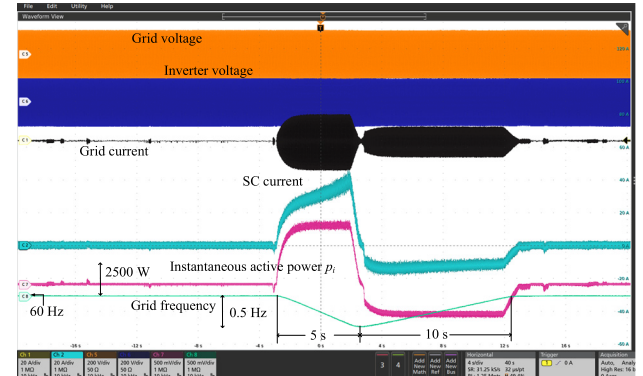


Fig. 15. Verification for the  $df/dt$ -based power control for the grid-forming SC inverter.

real grid with  $U_C = U_g = 390 \text{ V}$  (ph-ph rms voltage  $480 \text{ V}$ ),  $\omega_g = 120\pi$ , and  $X = 0.67854 \Omega$ . The poles are selected as  $p_1 = p_2 = 1$ , which results in  $k_{i\theta} = 6.2075e-06 \text{ kg}^{-1} \cdot \text{m}^{-2} \cdot \text{s}^2$ ,  $k_{i\omega} = 3.1037e-06 \text{ kg}^{-1} \cdot \text{m}^{-2} \cdot \text{s}$ ,  $k_{rp} = -3.1037e-06 \text{ kg}^{-1} \cdot \text{m}^{-2} \cdot \text{s}^2$ ,  $J_{PVSG} = 1/(\omega_n k_{i\omega}) = 854 \text{ kg} \cdot \text{m}^2$ . The selected  $J_{PVSG}$  is relatively large, since the real grid frequency variation is very small, so is the RoCoF.

Fig. 17 shows a comprehensive experimental result for a long time of  $200 \text{ s}$ . All of the signals are labeled in the figure. The grid frequency, which is not used in the control loop, is derived from a frequency-locked loop for

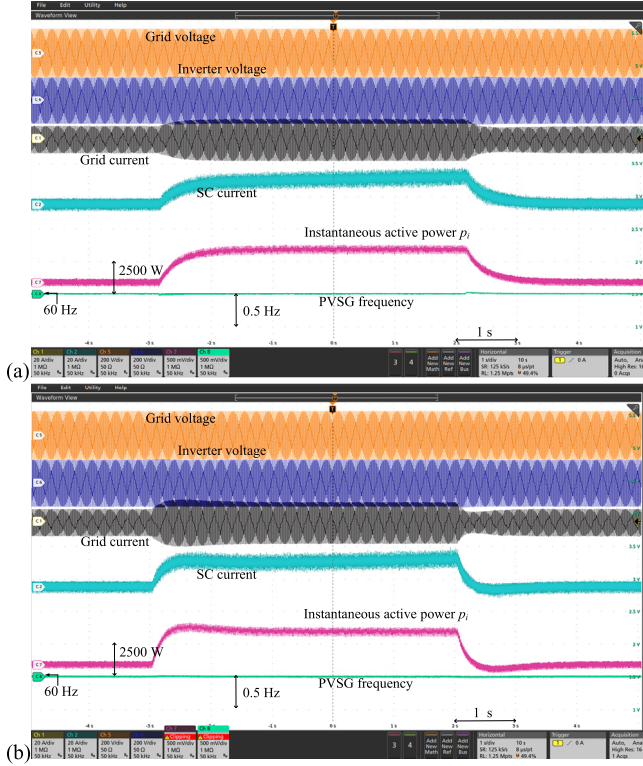


Fig. 16. Comparison results of the reference step between the (a) proposed power controller and (b) PI-based power controller.

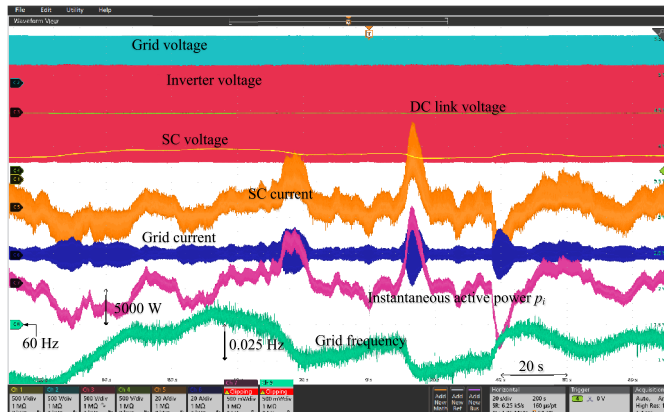


Fig. 17. PVSG experimental results when connected to the 480-V three-phase grid.

monitoring purposes. As shown by the pink curve (channel 7), the active instantaneous power of the inverter is dependent on the variation of the grid frequency denoted by the green curve (channel 8). If the grid frequency is increasing, the inverter will absorb active power from the grid, and vice versa. This means that the inverter attempts to resist the grid frequency variation. This is the inertia to prevent the grid frequency deviating from the current state. The value of the active power is proportional to the RoCoF. This also demonstrates that the faster the grid frequency changes; the larger power will be provided by the inverter. This is a good property for sustaining the grid frequency stability. The grid current shown by the blue curve verifies the inertia

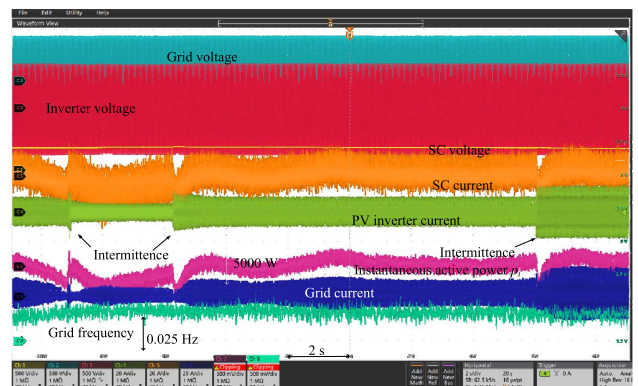


Fig. 18. PVSG experimental results of power filter for PV intermittence when connected to the 480-V three-phase grid.

power supplied by the inverter. The SC current and the SC voltage shown in Fig. 17 reflect the operation state of the inverter. All the results prove that the proposed solution works very well to provide the frequency inertia support for the grid.

Fig. 18 shows the experimental results of the power filter when there is PV intermittence. The conventional PV system consists of the PV emulator and the PV inverter as shown in Fig. 11. In Fig. 18, when the PV system has intermittence as shown by the bright green curve (channel 4), the SC inverter can absorb the step power immediately and then release the power slowly. Consequently, the grid power follows the PV power slowly in 1 s, as shown by the blue curve. Hence, the power filter for the PV intermittence is achieved. Furthermore, with the varying grid frequency, the PVSG still regulates the output power to support the grid frequency. It demonstrates that the proposed PVSG can successfully transform the grid-following PV system to a grid-forming VSG.

## VI. CONCLUSION

In this article, a grid-forming modification solution, which utilizes a paralleled SC inverter on the ac side, is proposed for the conventional PV system. It effectively transforms an existing PV system from a grid-following to grid-forming system PVSG without any change for the PV inverter itself. This ac coupled scheme greatly improves the reliability and reduces the cost for the modification. Two-stage converter topologies are used for the SC inverter. The dc-link voltage control and the ac voltage control form the fast power response function of the PVSG. A simple and effective power controller is designed to realize the inertia supply and power filter functions, and also the power tracking performance is improved. The frequency inertia always resists the grid frequency derivation by a  $df/dt$ -based power control. When the grid frequency decreases, the proposed grid-forming inverter injects active power to prevent frequency reduction and vice versa. If a pulsating power is generated by the paralleled PV intermittence, the proposed grid-forming inverter can serve as a power filter to automatically filter the pulsating power, so that the pulsating power impact of the grid is alleviated. All proposed functions are realized and verified experimentally. The proposed PVSG control can also be easily extended to provide the droop support (primary frequency response) when a battery is

used instead of the SC. The disadvantage of the proposed PVSG is that it requires a short electrical distance between the existing PV inverter and added SC inverter.

## REFERENCES

- [1] J. Rocabert, A. Luna, F. Blaabjerg, and P. Rodriguez, "Control of power converters in AC microgrids," *IEEE Trans. Power Electron.*, vol. 27, no. 11, pp. 4734–4749, Nov. 2012.
- [2] P. Piya, M. Ebrahimi, M. Karimi-Ghartemani, and S. A. Khajehoddin, "Fault ride-through capability of voltage-controlled inverters," *IEEE Trans. Ind. Electron.*, vol. 65, no. 10, pp. 7933–7943, Oct. 2018.
- [3] J. Fang, H. Li, Y. Tang, and F. Blaabjerg, "On the inertia of future more-electronics power systems," *IEEE J. Emerg. Sel. Topics Power Electron.*, vol. 7, no. 4, pp. 2130–2146, Dec. 2019, doi: [10.1109/JESTPE.2018.2877766](https://doi.org/10.1109/JESTPE.2018.2877766).
- [4] Y. G. Rebours, D. S. Kirschen, M. Trotignon, and S. Rossignol, "A survey of frequency and voltage control ancillary services—Part I: Technical features," *IEEE Trans. Power Syst.*, vol. 22, no. 1, pp. 350–357, Feb. 2007.
- [5] Q.-C. Zhong and G. Weiss, "Synchronverters: Inverters that mimic synchronous generators," *IEEE Trans. Ind. Electron.*, vol. 58, no. 4, pp. 1259–1267, Apr. 2011.
- [6] Y. Chen, R. Hesse, D. Turschner, and H.-P. Beck, "Investigation of the Virtual Synchronous Machine in the island mode," in *Proc. 3rd IEEE PES Innov. Smart Grid Technol. Eur. (ISGT Eur.)*, Berlin, Germany, Oct. 2012, pp. 1–6.
- [7] S. Dong and Y. C. Chen, "A method to directly compute synchronconverter parameters for desired dynamic response," *IEEE Trans. Energy Convers.*, vol. 33, no. 2, pp. 814–825, Jun. 2018.
- [8] S. Wang, J. Hu, and X. Yuan, "Virtual synchronous control for grid-connected DFIG-based wind turbines," *IEEE J. Emerg. Sel. Topics Power Electron.*, vol. 3, no. 4, pp. 932–944, Dec. 2015.
- [9] H. Wu *et al.*, "Small-signal modeling and parameters design for virtual synchronous generators," *IEEE Trans. Ind. Electron.*, vol. 63, no. 7, pp. 4292–4303, Jul. 2016.
- [10] Y. Deng, Y. Tao, G. Chen, G. Li, and X. He, "Enhanced power flow control for grid-connected droop-controlled inverters with improved stability," *IEEE Trans. Ind. Electron.*, vol. 64, no. 7, pp. 5919–5929, Jul. 2017.
- [11] X. Meng, J. Liu, and Z. Liu, "A generalized droop control for grid-supporting inverter based on comparison between traditional droop control and virtual synchronous generator control," *IEEE Trans. Power Electron.*, vol. 34, no. 6, pp. 5416–5438, Jun. 2019.
- [12] S. D'Arco and J. A. Suul, "Equivalence of virtual synchronous machines and frequency-droops for converter-based microgrids," *IEEE Trans. Smart Grid*, vol. 5, no. 1, pp. 394–395, Jan. 2014.
- [13] W. Zhang, A. M. Cantarellas, J. Rocabert, A. Luna, and P. Rodriguez, "Synchronous power controller with flexible droop characteristics for renewable power generation systems," *IEEE Trans. Sust. Energy*, vol. 7, no. 4, pp. 1572–1582, Oct. 2016.
- [14] W. Zhang *et al.*, "Comparison of different power loop controllers for synchronous power controlled grid-interactive converters," in *Proc. IEEE Energy Convers. Congr. Expo. (ECCE)*, Montreal, QC, Canada, Sep. 2015, pp. 3780–3787.
- [15] W. Zhang, D. Remon, and P. Rodriguez, "Frequency support characteristics of grid-interactive power converters based on the synchronous power controller," *IET Renew. Power Gener.*, vol. 11, no. 4, pp. 470–479, 2017.
- [16] W. Zhang, D. Remon, I. Candela, A. Luna, and P. Rodriguez, "Grid-connected converters with virtual electromechanical characteristics: Experimental verification," *CSEE J. Power Energy Syst.*, vol. 3, no. 3, pp. 286–295, Sep. 2017.
- [17] S. A. Khajehoddin, M. Karimi-Ghartemani, and M. Ebrahimi, "Grid-supporting inverters with improved dynamics," *IEEE Trans. Ind. Electron.*, vol. 66, no. 5, pp. 3655–3667, May 2019.
- [18] J. Fang, H. Li, Y. Tang, and F. Blaabjerg, "Distributed power system virtual inertia implemented by grid-connected power converters," *IEEE Trans. Power Electron.*, vol. 33, no. 10, pp. 8488–8499, Oct. 2018, doi: [10.1109/TPEL.2017.2785218](https://doi.org/10.1109/TPEL.2017.2785218).
- [19] L. Huang *et al.*, "A virtual synchronous control for voltage-source converters utilizing dynamics of DC-link capacitor to realize self-synchronization," *IEEE J. Emerg. Sel. Topics Power Electron.*, vol. 5, no. 4, pp. 1565–1577, Dec. 2017, doi: [10.1109/JESTPE.2017.2740424](https://doi.org/10.1109/JESTPE.2017.2740424).
- [20] J. Cao, W. Du, H. Wang, and M. McCulloch, "Optimal sizing and control strategies for hybrid storage system as limited by grid frequency deviations," *IEEE Trans. Power Syst.*, vol. 33, no. 5, pp. 5486–5495, Feb. 2018.
- [21] J. Fang, Y. Tang, H. Li, and X. Li, "A battery/ultracapacitor hybrid energy storage system for implementing the power management of virtual synchronous generators," *IEEE Trans. Power Electron.*, vol. 33, no. 4, pp. 2820–2824, Apr. 2018.
- [22] J. Rocabert, R. Capó-Misut, R. S. Muñoz-Aguilar, J. I. Candela, and P. Rodriguez, "Control of energy storage system integrating electrochemical batteries and supercapacitors for grid-connected applications," *IEEE Trans. Ind. Appl.*, vol. 55, no. 2, pp. 1853–1862, Mar./Apr. 2019.
- [23] V. Gevorgian and B. O'Neill, "Advanced grid-friendly controls demonstration project for utility-scale PV power plants," NREL, Golden, CO, USA, Tech. Rep. NREL/TP-5D00-65368, Jan. 2016.
- [24] A. F. Hoke, M. Shirazi, S. Chakraborty, E. Muljadi, and D. Maksimovic, "Rapid active power control of photovoltaic systems for grid frequency support," *IEEE J. Emerg. Sel. Topics Power Electron.*, vol. 5, no. 3, pp. 1154–1163, Sep. 2017, doi: [10.1109/JESTPE.2017.2669299](https://doi.org/10.1109/JESTPE.2017.2669299).
- [25] E. Shoubaki, S. Essakiappan, M. Manjrekar, and J. Enslin, "Synthetic inertia for BESS integrated on the DC-link of grid-tied PV inverters," in *Proc. IEEE 8th Int. Symp. Power Electron. Distrib. Gener. Syst. (PEDG)*, Florianopolis, Brazil, Apr. 2017, pp. 1–5.
- [26] D. Chen, Y. Xu, and A. Q. Huang, "Integration of DC microgrids as virtual synchronous machines into the AC grid," *IEEE Trans. Ind. Electron.*, vol. 64, no. 9, pp. 7455–7466, Sep. 2017.
- [27] H. Shi, F. Zhuo, H. Yi, F. Wang, D. Zhang, and Z. Geng, "A novel real-time voltage and frequency compensation strategy for photovoltaic-based microgrid," *IEEE Trans. Ind. Electron.*, vol. 62, no. 6, pp. 3545–3556, Jun. 2015.
- [28] D. Duckwitz and B. Fischer, "Modeling and design of df/dt-based inertia control for power converters," in *IEEE J. Emerg. Sel. Topics Power Electron.*, vol. 5, no. 4, pp. 1553–1564, Dec. 2017.
- [29] J. Fang, R. Zhang, H. Li, and Y. Tang, "Frequency derivative-based inertia enhancement by grid-connected power converters with a frequency-locked-loop," *IEEE Trans. Smart Grid*, vol. 10, no. 5, pp. 4918–4927, Sep. 2019.
- [30] B. W. Bequette, *Process Control: Modeling, Design and Simulation*. Zug, Switzerland: Pearson Schweiz Ag, 2003.
- [31] T. Kailath, *Linear Systems*. Englewood Cliffs, NJ, USA: Prentice-Hall, 1980, ch. 3, pp. 201–202.
- [32] X. Quan, X. Dou, Z. Wu, M. Hu, H. Song, and A. Q. Huang, "A novel dominant dynamic elimination control for voltage-controlled inverter," *IEEE Trans. Ind. Electron.*, vol. 65, no. 8, pp. 6800–6812, Aug. 2018.
- [33] X. Quan, X. Zhao, L. Zhang, R. Xu, Y. Lei, and A. Q. Huang, "Novel power control of voltage-controlled inverters for grid inertia support," in *Proc. IEEE Appl. Power Electron. Conf. Expo. (APEC)*, Anaheim, CA, USA, Mar. 2019, pp. 927–931.
- [34] M. G. Taul, X. Wang, P. Davari, and F. Blaabjerg, "Current limiting control with enhanced dynamics of grid-forming converters during fault conditions," *IEEE J. Emerg. Sel. Topics Power Electron.*, to be published.
- [35] M. Karimi-Ghartemani, S. A. Khajehoddin, P. Piya, and M. Ebrahimi, "Universal controller for three-phase inverters in a microgrid," *IEEE J. Emerg. Sel. Topics Power Electron.*, vol. 4, no. 4, pp. 1342–1353, Dec. 2016.



**Xiangjun Quan** (S'16–M'18) received the B.S.E.E. degree in power systems and its automation from Chongqing University, Chongqing, China, in 2007, and the M.S. degree in power systems and its automation and the Ph.D. degree from Southeast University, Nanjing, China, in 2014 and 2018, respectively.

He studied in FREEDM with North Carolina State University, Raleigh, NC, USA, from February 2017 to August 2017. From September 2017 to August 2018, he also studied at the University of Texas at Austin, Austin, TX, USA, as an Exchange Student. He was a Research and Development Engineer with Shanghai Research Development Department of Renewable Energy, Huawei Technologies, from 2011 to 2012. Since 2018, he has been an Assistant Professor with Southeast University, and also with the Semiconductor Power Electronics Center (SPEC) as a Researcher with the University of Texas at Austin. His current research interests include digital control techniques for converters, renewable energy generation systems, and microgrids.



**Ruiyang Yu** received the B.E. degree in electrical engineering from Shandong University, Jinan, China, in 2007, and the M.S. and Ph.D. degrees in power electronics from The University of Hong Kong, Hong Kong, in 2008 and 2013, respectively.

He was a Post-Doctoral Research Fellow from 2013 to 2017 and an Instructor in 2016 with North Carolina State University, Raleigh, NC, USA. He is currently a Research Associate with The University of Texas at Austin, Austin, TX, USA. His research interests include high-frequency and power-density power converter designs, megawatt power converter design, magnetic component designs, and power converter control.



**Chengjing Li** (S'17) received the B.S.E.E. degree from Harbin Engineering University, Harbin, China, in 2015, and the M.Sc. degree from the Huazhong University of Science and Technology, Huazhong, China, in 2018.

He is currently a Graduate Student with the Semiconductor Power Electronics Center (SPEC), University of Texas at Austin, Austin, TX, USA. His current research interests include multi-level converters, renewable energy generation systems, and microgrids.



**Xin Zhao** received the B.S.E.E. degree in electronic packaging technology and the M.S. degree in materials engineering from the Harbin Institute of Technology, Harbin, China, in 2012 and 2014, respectively, and the M.S. degree in electrical engineering from North Carolina State University, Raleigh, NC, USA, in 2017. He is currently pursuing the Ph.D. degree in power electronics with the University of Texas at Austin, Austin, TX, USA.

His current research interests include medium-voltage solid-state transformers, high-density integration of power supply, and power electronics packaging.



**Yang Lei** received the B.S. degree in electrical engineering from the Huazhong University of Science and Technology, Wuhan, China, in 2011, and the M.S. degree in electrical engineering from North Carolina State University, Raleigh, NC, USA, in 2014. He is currently pursuing the Ph.D. degree in electrical engineering with the University of Texas at Austin, Austin, TX, USA.



**Alex Q. Huang** (S'91-M'94-SM'96-F'05) was born in Zunyi, Guizhou, China. He received the B.Sc. degree from Zhejiang University, Zhejiang, China, in 1983, the M.Sc. degree from the Chengdu Institute of Radio Engineering, Chengdu, China, in 1986, both in electrical engineering, and the Ph.D. degree in electrical engineering from Cambridge University, Cambridge, U.K., in 1992.

From 1992 to 1994, he was a Research Fellow with the Magdalene College, Cambridge. From 1994 to 2004, he was a Professor with the Bradley Department of Electrical and Computer Engineering, Virginia Polytechnic Institute and State University, Blacksburg, VA, USA. From 2004 to 2017, he was the Progress Energy Distinguished Professor of Electrical and Computer Engineering with NC State University, Raleigh, NC, USA, where he established and led the NSF FREEDM Systems Center. Since 2017, he has been the Dula D. Cockrell Centennial Chair in Engineering with the University of Texas at Austin, Austin, TX, USA. Since 1983, he has been involved in the development of modern power semiconductor devices and power integrated circuits. He fabricated the first IGBT power device in China in 1985. He is the Inventor and Key Developer of the emitter turn-off (ETO) thyristor. He developed the concept of Energy Internet and the smart transformer-based Energy Router technology. He has mentored and graduated more than 80 Ph.D. and master's students and authored or coauthored more than 500 articles in international conferences and journals. He has also been granted more than 20 U.S. patents. His current research interests are power electronics, power management microsystems, and power semiconductor devices.

Dr. Huang is a fellow of the National Academy of Inventors (NAI). He was a recipient of the NSF CAREER award, the prestigious Research and Development 100 Award, the MIT Technology Review's 2011 Technology of the Year Award, and the 2019 IEEE IAS Gerald Kliman Innovator Award.



**Tianxiang Chen** (S'17) was born in Hangzhou, China. He received the B.Eng. degree from the Harbin Institute of Technology, Harbin, China, in 2015, and the M.S. degree from North Carolina State University, Raleigh, NC, USA, in 2017, both in electrical engineering. He is currently pursuing the Ph.D. degree with the Semiconductor Power Electronics Center, University of Texas at Austin, Austin, TX, USA.

His research interests include the design, control, and optimization of high density and high-frequency power converters.